Journal of Materials Chemistry A

Enabling Stable and High-Rate Cycling of Ni-Rich Layered Oxide Cathode for Lithium-Ion Batteries by Modification with an Artificial Li^+-Conducting Cathode-Electrolyte Interphase

Journal:	*Journal of Materials Chemistry A*
Manuscript ID	TA-ART-03-2021-002563.R1
Article Type:	Paper
Date Submitted by the Author:	10-Apr-2021
Complete List of Authors:	Wang, Shixuan; Wuhan University Dai, Alvin ; Argonne National Laboratory Cao, Yuliang; Wuhan University, Department of Chemistry Yang, Han; Wuhan university, Chemistry Amine, Khalil; Argonne National Laboratory, Lu, Jun; Argonne National Laboratory, Chemical Science and Engineering Division Li, Hui; Wuhan University, Ai, Xinping; Wuhan University, Chemistry

ARTICLE

Enabling Stable and High-Rate Cycling of Ni-Rich Layered Oxide Cathode for Lithium-Ion Batteries by Modification with an Artificial Li^+-Conducting Cathode-Electrolyte Interphase †

Received 00th January 20xx,
Accepted 00th January 20xx

DOI: 10.1039/x0xx00000x

Shixuan Wang[a], Alvin Dai[b], Yuliang Cao[a], Hanxi Yang[a], Amine Khalil[b], Jun Lu[b]*, Hui Li [a]*, Xinping Ai[a]*

Ni-rich $LiNi_{0.8}Co_{0.1}Mn_{0.1}O_2$ (NCM811) cathodes are investigated to realize high energy density Li ion batteries for long life electric vehicle applications. However, capacity decay and thermal instability due to cathode-electrolyte interfacial degradation remain challenges that require sophisticated surface stabilization methods to address. Here, we propose a strategy, for the first time, to form an artificial Li^+-conducting cathode-electrolyte interphase (ALCEI) on the NCM811 cathode surface using a nucleophilic reaction between polysulfides and vinylene carbonate (VC). The as-formed ALCEI layer simultaneously protects the NCM particles from electrolyte corrosion and facilitates Li^+ ion transport, thus enabling stable and high rate cycling of NCM811. As a result, the ALCEI-modified NCM811 cathode exhibits a high capacity (211.6 mAh g^{-1} at 0.1C), notable rate capability (134 mAh g^{-1} at 10C), and superior cycle stability (94.2% over 200 cycles at 1C). These results underscore the use of interfacial engineering in high voltage cathode material development and provides a feasible strategy for stabilizing Ni-rich cathode interfaces in practical Li ion battery applications.

1. Introduction

Owing to their high specific capacities and low cost, Ni-rich lithium layered oxides with high Ni contents such as $LiNi_{0.8}Co_{0.1}Mn_{0.1}O_2$ (NCM) or $LiNi_{0.8}Co_{0.15}Al_{0.05}O_2$ (NCA) are highly desired and developed as a promising cathode for next-generation lithium ion batteries (LIBs).[1-7] However, obtaining higher capacities in these Ni-rich materials comes at the cost of cycle and thermal stability, due to an increase in unstable Ni-O bonds that destabilize the lattice structure and increase surface reactivity during cycling.[8-11] As reported,[12-15] nickel-rich cathodes undergo surface degradation at highly delithiated states due to chemical reactions between Ni^{4+} and solvents in electrolyte that promote transition metal dissolution and NiO-like rock-salt phase formations. The as formed, Li^+-deficient, and impermeable rock-salt phase impedes Li^+ diffusion transport between the bulk lattice and electrolyte, thus increasing interfacial reaction resistance at the cathode.[16, 17] Moreover, the parasitic surface reaction exacerbates morphological and structural damage in nickel-rich materials, which promotes electrolyte penetration into secondary particle interiors and subsequent reactions with primary crystallites. This parasitic reaction propagates throughout the grain boundaries of the secondary particles and accelerates lattice microcracking that leads to structural distortion and cathode capacity loss.[18-20]

Various strategies to alleviate this parasitic side reaction and stabilize the interfacial structure of nickel-rich cathodes have been proposed, including robust cathode-electrolyte interphase (CEI), [12, 17, 21, 22] elemental doping of bulk lattice,[23-25] morphological/structural tailoring,[26-28] or electrolyte optimization. [29-31] Among these methods, building a stable CEI is a direct way to shield Ni-rich material surfaces from electrolyte corrosion and inhibit surface parasitic reactions. A number of chemically and electrochemically stable metal oxides (e.g., TiO_2, ZrO_2 and Al_2O_3),[32-34] fluorides (e.g., LiF and AlF_3),[35, 36] and phosphates (e.g., $Mn_3(PO_4)_2$ and $AlPO_4$) [37, 38] have already been used as an artificial CEI to modify the surface of Ni-rich NCM or NCA materials through various wet chemical processes. Asides from their complicated synthetic processes, these coated CEI layers provide poor Li^+ conductivity that is detrimental to cathode rate capability. Recent work has attempted to resolve this problem by coating the Ni-rich materials with Li^+ conductive phases that include Li_3PO_4,[39, 40] $LiFePO_4$,[41, 42] or $Li_{1.3}Al_{0.3}Ti_{1.7}(PO_4)_3$ [43]. However, these inorganic layers are brittle, easily fractured, and detach from the particle surface during anisotropic lattice volume changes that occur due to Li-insertion/extraction in Ni-rich layered compounds. Compared to inorganic CEI layers, conducting polymers (e.g., polyaniline (PANI), polythiophene (PTPh) and polypyrrole (PPy))[44-46] have good structural flexibility and are capable of accommodating cathode material volume changes as a conformal CEI layer. However, these conducting polymers usually swell and are slightly soluble in organic electrolytes, which makes it difficult to form completely homogeneous and dense surface layers. Therefore, building a

[a] Hubei Key Lab of Electrochemical Power Sources, College of Chemistry & Molecular Science, Wuhan University, Wuhan, 430072, China. E-mail address: xpai@whu.edu.cn
[b] Chemical Sciences and Engineering Division, Argonne National Laboratory, Lemont, IL 60439, USA. E-mail address: junlu@anl.gov

†Electronic Supplementary Information (ESI) available: The detailed vibration modes and assignments of the IR absorption bands of ALCEI; Possible reaction routes of polysulfides with VC molecules; TG curves of pristine and ALCEI-modified NCM811 in air; CV curves of pristine and ALCEI-modified NCM811 cathodes; Variations of mean discharge voltage for both the pristine and ALCEI-modified NCM811 cathodes with cycling numbers; SEM and TEM images of the cathodes after 40 cycles; Video for VC solvent reacting with Li_2S_8 solution. See DOI: 10.1039/x0xx00000x

chemically inert and Li^+-conductive CEI to stabilize the interfacial chemistry of Ni-rich NCM (or NCA) cathode is essential for realizing high energy applications.

In this work, we propose an original and facile strategy to build an artificial Li^+-conducting cathode-electrolyte interphase (ALCEI) on the surface of NCM811 cathodes using a nucleophilic reaction between polysulfides in an ether solvent and vinylene carbonate (VC) molecules pre-adsorbed on the NCM particles. The as formed ALCEI layer is robust, electrochemically stable, and has high Li^+ conductivity. These properties shield the NCM particles from direct contact with electrolyte and promote Li^+ ion transfer between the bulk lattice and electrolyte, thus creating a chemically stable and electrochemically favorable interface for the NCM cathode. The ALCEI-modified NCM811 cathode subsequently exhibits improved capacity, superior rate capability, and significantly enhanced cyclability when compared to its pristine counterpart. These promising results demonstrate a viable method to realize cycle stability and high-rate capability in Ni-rich cathodes for Li ion battery applications.

2. Experimental

2.1 Materials synthesis

ALCEI-modified NCM811 was obtained through a nucleophilic reaction of polysulfide Li_2S_8 with carbonate solvent, vinylene carbonate (VC). Initially, 1.0 g of NCM811 powder (Lishen Ltd., China) was added to a 200 μL VC/ether co-solvent electrolyte under vigorous stirring. The VC/ether co-solvent electrolyte was prepared by dissolving 1 mol L^{-1} lithium bis-trifluoromethanesulfonimide (LiTFSI) in a mixture of VC (Aladdin, China), DME and 1, 3-dioxolane (DOL, DodoChem, China) solvent with a volume ratio of 1.0: 4.5: 4.5. After evaporation to remove ether solvents, the residual VC molecules and LiTFSI salt were homogeneously deposited on the inner/outer surfaces of NCM811 powders. As formed NCM811 powders were then transferred to a 1.25 mL Li_2S_8 solution and constantly stirred for 6h to complete the nucleophilic reaction. The Li_2S_8 solution was stoichiometrically prepared by dissolving sublimed sulfur (Aladdin, China) and Li_2S (Aladdin, China) at a molar ratio of 7:1 in a dimethoxyethane solvent (DME, J&K Scientific Ltd., China). After completion of the nucleophilic reaction, the NCM particles were filtered, washed with DME solvent, and vacuum-dried at 100 ºC to obtain the ALCEI-coated NCM811 material.

To facilitate chemical and conductivity analysis, a larger quantity of ALCEI powder was obtained by direct nucleophilic reaction of Li_2S_8 solution with VC co-solvent electrolyte at a volume ratio of 2:5. After completion of the reaction, the products were collected by filtration, washed with DME, vacuum-dried at 100 ºC, and then used as an analogue compound of ALCEI for physical characterization.

2.2 Structural characterization

Chemical composition of ALCEI, the reaction product of Li_2S_n and VC, was analyzed by Fourier Transform Infrared Spectrometry (FT-IR, Nicolet iS50, USA). The crystalline structures of pristine and ALCEI-modified NCM811 materials were characterized by X-ray diffraction (XRD, Rigaku Miniflex600, Japan). Field emission scanning electron microscope (FE-SEM, ZEISS Merlin Compact VP, Germany) and high-resolution transmission electron microscopy (HRTEM, JEOL JEM 2100, Japan) were used to observe the morphological changes of the NCM811 materials before and after surface modification as required. Brunauer–Emmett–Teller (BET) method was utilized to determine the specific surface area of NCM811 materials. The surface chemical states of pristine and modified NCM811 materials were detected by X-ray photoelectron spectroscopy (XPS, ThermoFischer EscaLab Xi+, USA). The mass content of the ALCEI layer on the cathode material was measured by thermogravimetric analysis (TGA, Mettler-Toledo TGA2 / DSC3, Switzerland) with a heating rate of 10 ºC min^{-1} from 100 to 650 ºC in air atmosphere.

2.3 Electrochemical characterization

ALCEI ionic conductivity was measured by electrochemical impedance spectroscopy (EIS) and conducted on an electrochemical working station (Autolab PGSTAT128N, Eco Chemie, Netherlands) over a frequency range from 1 Hz to 10^5 Hz with an amplitude of 10 mV. The solid product was first pressed into a compact disk and then sandwiched between two stainless-steel blocking electrodes for impedance measurement. The electrochemical stability of the reaction product was measured by linear sweep voltammetry (LSV), carried out on a CHI660a electrochemical workstation at a scan rate of 0.1 mV s^{-1} in the potential range from 3.0 to 4.5 V (vs Li/Li^+). For LSV measurement, the ALCEI powder was coated on a super P electrode to ensure a good electrical contact. Electrochemical performances of NCM cathode materials were tested in CR2016 coin-type cells with a Li disk as counter electrode and a polyethylene microporous membrane as separator. The cathode electrodes were fabricated by mixing active material (pristine or ALCEI-modified NCM811), conductive carbon (Super P), and polyvinylidene fluoride binder (PVDF, Macklin) at a weight ratio of 8:1:1 in a N-methyl pyrrolidone solvent (NMP, Aladdin) to form a uniform slurry, and then coating the slurry on an Al foil substrate. After vacuum-drying at 80 ºC for 5 h, the electrode film was cut into φ=12 mm disks with an active material loading of about 3.0 mg cm^{-2}. The electrolyte used in this work was 1 M $LiPF_6$ solution in dimethyl carbonate (DMC) /ethylene carbonate (EC) /ethyl methyl carbonate (EMC) (1:1:1 by vol.), purchased from DodoChem, China. Galvanostatic charge-discharge measurements were carried out on a Neware battery testing system (CT-4008) within a voltage range of 2.7-4.3 V (vs Li/Li^+) at 25 ºC. CV and EIS measurements were performed on a CHI660a electrochemical working station. CV measurement was carried out with a scan rate of 0.2 mV s^{-1} within the voltage range of 3.0-4.4 V (vs Li/Li^+). EIS analysis was performed over the frequency range from 0.01 Hz to 10^5 Hz with an amplitude of 10 mV.

3. Results and discussion

In previous work on Li/S batteries,[47] we found that VC molecules can nucleophilically react with Li_2S_8 intermediate at a very fast rate to deposit a CEI film on the sulfur electrode surface, and the as-formed CEI film can inhibit electrolyte penetration while allowing Li^+ diffusion, thus ensuring stable cycling of sulfur cathode. Inspired by this finding, we designed a nucleophilic reaction to build a suitable ALCEI layer on nickel-rich NCM cathode using Li_2S_8 and VC molecules. As shown by the supplementary video, the VC solvent rapidly reacts with the Li_2S_8 solution and is accompanied by an immediate color change from colorless to wine red. Possible reaction routes are displayed in Figure

S1. Figure 1 illustrates the synthetic process for ALCEI-modified NCM811 material. First, NCM811 powders are thoroughly infiltrated with a VC/ether co-solvent electrolyte (1 M LiTFSI/VC-DME-DOL). Under continuous stirring, the low boiling ether solvents are evaporated with the residue of VC and LiTFSI salt remaining on the inner and outer surfaces of NCM811 particles. The as formed NCM811 particles are then transferred to a Li_2S_8/DME solution, where VC molecules are nucleophilically reacted with Li_2S_8 to deposit a compact and thin ALCEI layer on NCM811 particles.

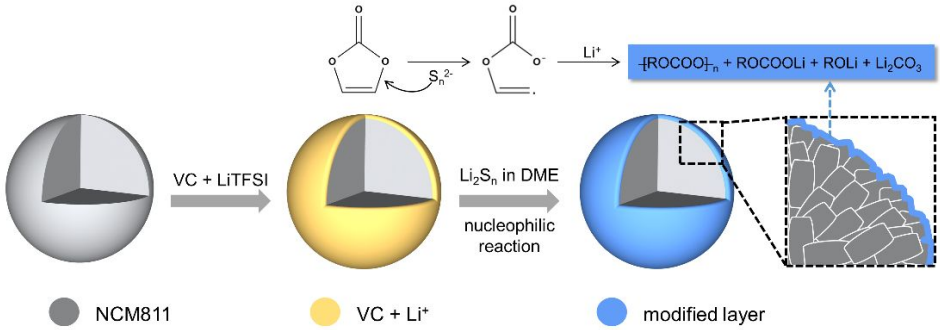

Fig. 1 Schematic illustration for the fabrication process of ALCEI-modified NCM811 material

However, the as formed ALCEI layer must satisfy several rigorous requirements when used on NCM811 that include electrochemical stability at high potentials, chemical tolerance toward highly oxidative $Ni^{+3/+4}$, high Li^+ conductivity, and mechanical robustness. To evaluate its applicability for NCM cathode, the ALCEI material was collected from the solid reaction product of Li_2S_8 and VC in solution and used for compositional, structural and electrochemical characterizations. Figure 2a shows the Ohmic impedance measured by electrochemical impedance spectroscopy (EIS) at room temperature for a circular piece of ALCEI sandwiched between two stainless-steel blocking electrodes. The EIS spectrum appears as a sloped line and its intercept on the real axis corresponds to the bulk resistance (R_b). Ionic conductivity can be calculated from the equation $\sigma = t/(R_b A)$, in which t and A are the thickness and area of the ALCEI sample, respectively.[48] From these calculations the ALCEI material has a room temperature ionic conductivity of 0.16 mS cm^{-1}, which is sufficient for fast Li^+ transport rates across a solid electrolyte interphase during insertion/extraction to and from the bulk NCM lattice.

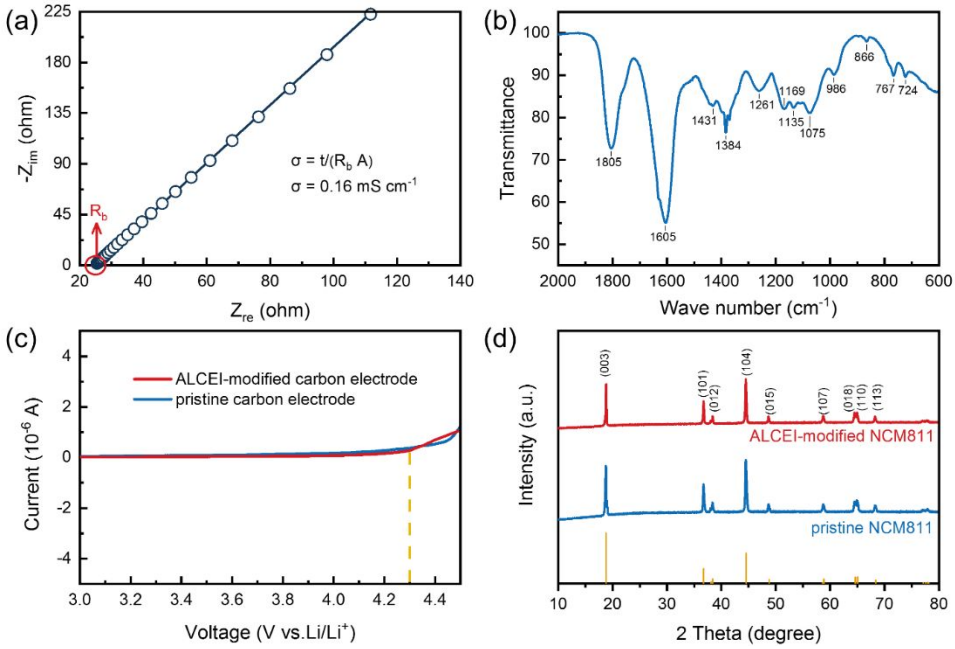

Fig. 2 Structural and electrochemical characterizations of ALCEI material: (a) EIS plot of the ALCEI sample sandwiched between two stainless steel blocking electrodes; (b) FT-IR spectrum; (c) LSV curves of the pristine and ALCEI-modified carbon electrodes in 1 M $LiPF_6$ EC/DMC/EMC (1:1:1 by vol.); (d) XRD patterns of pristine and ALCEI-modified NCM811.

Figure 2b exhibits FT-IR features of the ALCEI material. The IR peaks at 1805, 1261, 1169, and 1075 cm^{-1} are characteristic stretching vibrations of C=O, C-O, symmetrical and asymmetrical C-O-C in polycarbonates, whereas the peaks at 1605 and 1431 cm^{-1} reflect the stretching vibrations of C=O and C-O in lithium alkyl carbonates. In addition, the peak at 866 cm^{-1} corresponds to Li-O deformation vibrations in Li_2CO_3 or lithium alkyl oxides. The rest of the peaks are all related to methyl groups and methylene chains. The detailed vibration modes and assignments of the IR absorption bands are listed in Table S1.[49, 50] These FT-IR analyses reveal that the ALCEI material is composed of well-mixed polycarbonates, Li_2CO_3, lithium alkyl carbonates and lithium alkyl oxides, which are very similar to the components of the solid electrolyte interphase (SEI) formed on Li ion battery anodes. Due to this similarity in the chemical composition, the ALCEI layer is expected to behave like a SEI film to prevent parasitic electrolyte decomposition and stabilize battery operation.

The electrochemical window was measured by linear sweep voltammetry (LSV) in 1 M $LiPF_6$ EC/DMC/EMC to evaluate the oxidation tolerance of the ALCEI material. As shown in Figure 2c, no discernible current can be observed from the ALCEI-modified carbon electrode until the potential positively scans to 4.3 V, implying that the ALCEI can withstand a high positive potential without any discernible oxidation at 4.3 V. Such a wide electrochemical window enables the ALCEI layer to be stable on the NCM811 cathode at normal working potentials. Furthermore, to examine the chemical compatibility of the ALCEI with NCM811, XRD patterns of pristine and ALCEI-modified NCM811 materials were obtained.

As exhibited in Figure 2d, all diffraction peaks from these two samples are near identical and can be indexed to a well-developed rhombohedral $R\bar{3}m$ structure that is standard for layered NCM811. This means that the crystalline structure of the NCM811 remains intact after surface modification, or in other words, the nucleophilic reaction does not result in any etching or erosion of NCM811 in the modification process. Besides, the ALCEI layer shows no diffraction signals in the XRD pattern, possibly due to its amorphous structure or low content. The results discussed above highlight ALCEI material as having desirable Li ion conductivity as well as electrochemical and chemical compatibility, all of which are beneficial for creating stable NCM811 cathode interphases.

The morphologies of pristine and surface modified NCM811 were characterized using SEM and TEM. As displayed in Figure 3a and 3b, the pristine NCM811 appears as a spherical aggregate with a diameter of approximately 20 µm. These aggregates are composed of submicron-sized primary particles with 300-500 nm diameters. In comparison, the ALCEI-modified NCM811 keeps the same morphology but has rough surfaces decorated with smaller particles (Figure 3c and 3b), reflective of a refined modification layer. This thin ALCEI layer can be visualized from the TEM images in Figure 3e-3h. As can be seen, the pristine sample has a clear grain boundary without gradient surface layers (Figure 3e). On the contrary, the ALCEI-modified sample shows a distinct coating layer in the surface region (Figure 3f) and even at the contact area of two primary particles (Figure 3g), suggesting that NCM811 particles are fully coated with the ALCEI layer. From the TEM image of Figure 3d, it can be seen that such an ALCEI layer is uniformly distributed with a thickness of only ~ 7 nm, which does not significantly increase mass loading and minimally affects cathode specific energy density. The lattice fringe in the core of the ALCEI-modified sample has an interplanar distance of 0.472 nm for the characteristic (003) spacing plane of NCM811, which corresponds with XRD results that NCM811 lattice structures are unaffected during chemical modification.

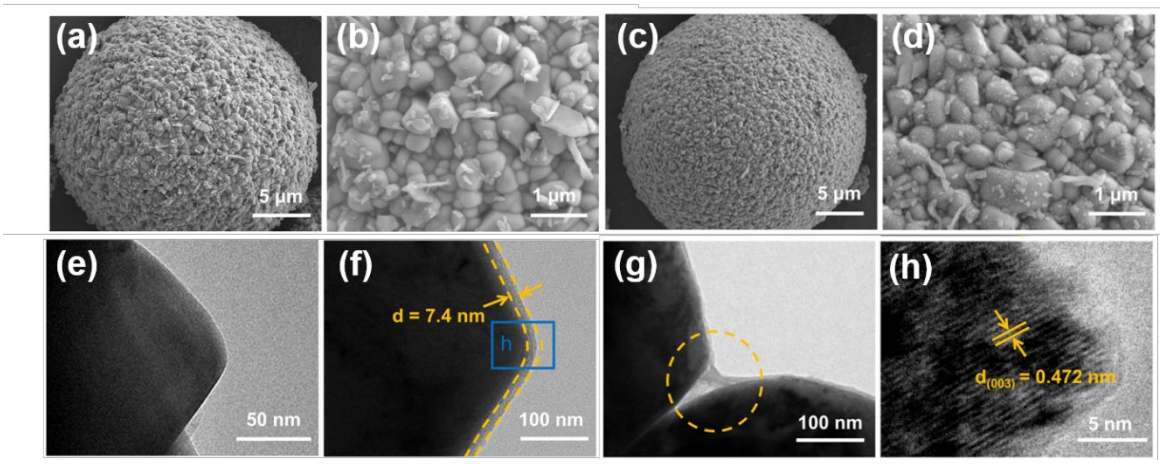

Fig. 3 SEM images of (a, b) pristine and (c, d) ALCEI-modified NCM811; TEM images of (e) pristine and (f-h) ALCEI-modified NCM811.

BET measurements further confirm that the ALCEI layer is modified not only on the outer surfaces but also onto surfaces deep

inside of NCM811 aggregates. The specific surface area and pore volume for pristine NCM811 are 0.467 m^2 g^{-1} and 0.0084 cm^3 g^{-1}, which changes to 0.319 m^2 g^{-1} and 0.0110 cm^3 g^{-1}, respectively, for the ALCEI-modified sample, indicating that this chemical modification can infiltrate deep inside the cathode particles. The total ALCEI mass content of 1.9%, derived from TGA analysis (Figure S2) also indicates minimal effects on cathode specific energy density.

XPS provides further information about the surface chemistry of the modified NCM811sample. As shown in Figure 4a, the XPS signals of Ni 2p, Co 2p, and Mn 2p appear from pristine NCM811 but disappear from the modified NCM811, reflecting a complete coverage of ALCEI layer on the NCM811 surface. The consistent appearing of O 1s signal is due to the presence of elemental oxygen in reaction products. Despite the O 1s signal, the C 1s, and Li 1s signals can also be detected on the surface of modified NCM811, which is entirely different from the pristine sample. As shown in Figure 4b, the C 1s spectrum exhibits five peaks, which can be attributed to the C 1s electron binding energies in -OCOO- of polycarbonates (289.88 eV), Li_2CO_3 (288.99 eV), ROCOOLi (288.72 eV), O-C bond (286.15 eV), and C-C bond (284.78 eV). In agreement with C 1s XPS signals, the fitted O 1s spectrum in Fig. 4c shows the presence of the O-C bond (533.40 eV), O=C bond (531.98 eV), Li_2CO_3 (531.83 eV), and ROLi (531.08 eV) in the modified layer. Besides, the Li 1s spectrum in Figure 4d can be well fitted with the Li 1s binding energies of ROCOOLi (55.87 eV), Li_2CO_3 (55.28 eV), and ROLi (54.63 eV). This XPS analysis demonstrates that the ALCEI layer is mainly composed of polycarbonates, lithium alkyl carbonates, lithium alkyl oxides, and Li_2CO_3, which is consistent with the FT-IR results.

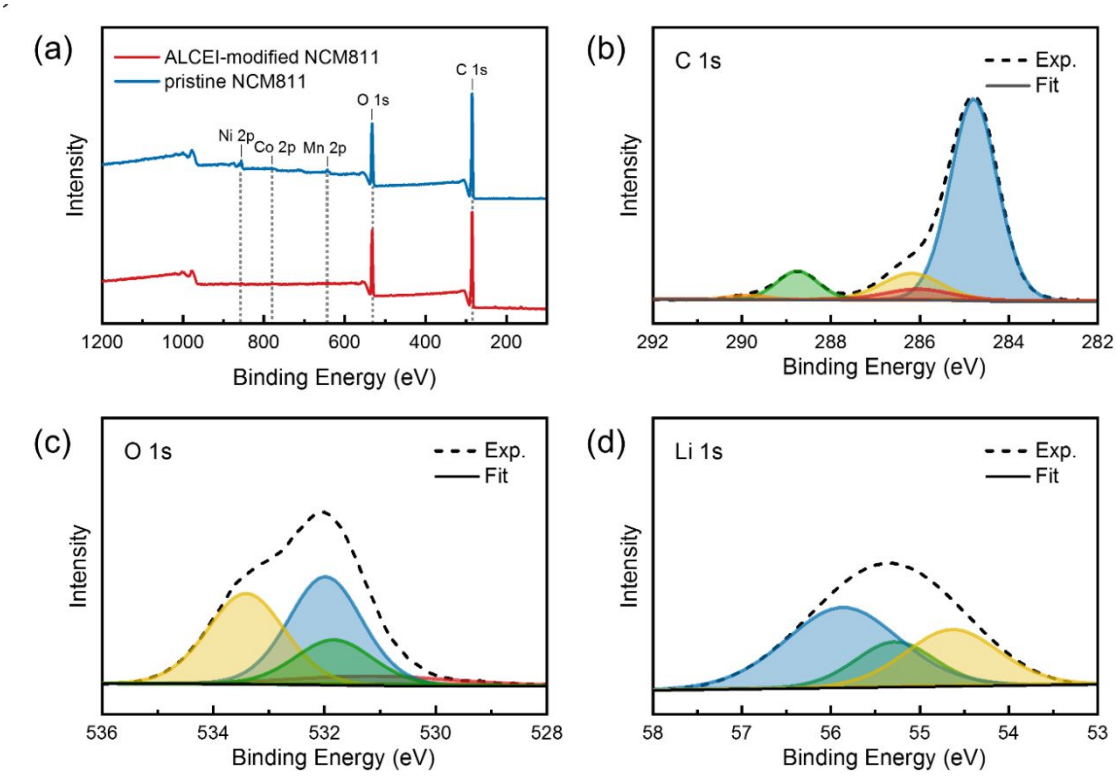

Fig. 4 (a) XPS surveys of pristine and ALCEI-modified NCM811. XPS spectrum of ALCEI-modified NCM811: (b) C 1s, (c) O 1s and (d) Li 1s.

Coin-type cells using pristine and ALCEI-modified NCM811 cathodes were assembled in parallel for electrochemical characterization to evaluate the functions of the ALCEI layer during cycling. The CV features of these two cathodes are given in Fig. S3. In the initial scan, both electrodes exhibit a huge anodic peak starting from 3.8 V and two unsymmetric cathodic peaks at 4.2V and 3.7V, respectively, due to the formation of a cathode-electrolyte interface (CEI) film and electrochemical activation during the initial delithiation process.[51] In subsequent scans, three pairs of reversible peaks appear in the CV curves, representing a continuous phase transition of NCM811: from hexagonal to monoclinic (H1-M), monoclinic to hexagonal (M-H2) and hexagonal to hexagonal (H2-H3) structure, respectively.[52] Nevertheless, in comparison with pristine NCM811 cathode the ALCEI-modified electrode shows improved kinetics and redox reversibility as reflected by its narrower anodic peak and better overlapped cathodic peaks in the CV scans.

Figure 5a provides data for the first charge-discharge of pristine and ALCEI-modified NCM811 cathodes. While both of them display similar charge/discharge behaviors with a delithiation plateau at ~ 3.9V and lithiation plateau at ~ 3.7V, the ALCEI-modified cathode exhibits a greatly reduced polarization and a slightly larger capacity during cycling when compared to the pristine cathode. The charge/discharge capacities are 223.9/205.6 mAh g^{-1} for pristine cathode and 238.1/211.6 mAh g^{-1} for the modified cathode, respectively. Fig. 5b compares the 1C rate cycling performances of

these two cathodes, measured after an initial electrochemical activation cycle. The reversible capacity of the pristine cathode decreases from its initial value of 179.1 mA h g^{-1} to 121.8 mA h g^{-1} over 300 cycles, corresponding to a retention of only 68%. In contrast, the ALCEI-modified cathode demonstrates a significantly enhanced cycling stability with reversible capacity decreasing slowly from 177.4 to 164.5 mA h g^{-1} during 300 cycles, achieving an impressively high-capacity retention of 92.7%. Besides, the modified cathode also exhibits a much more stable discharge plateau than its pristine counterpart. As shown in Figure S4, the modified cathode keeps its mean discharge voltage stable at 3.8 V during the entire 100 cycles, whereas the pristine cathode shows a 100 mV decrease in its discharge voltage due to gradual surface degradation occurring during cycling. This surface degradation most likely arises from irreversible phase transition of the surface structure induced by electrolyte etching, which produces an inactive NiO-like rock-salt phase to block Li^+ ion diffusion and increase interfacial resistance.

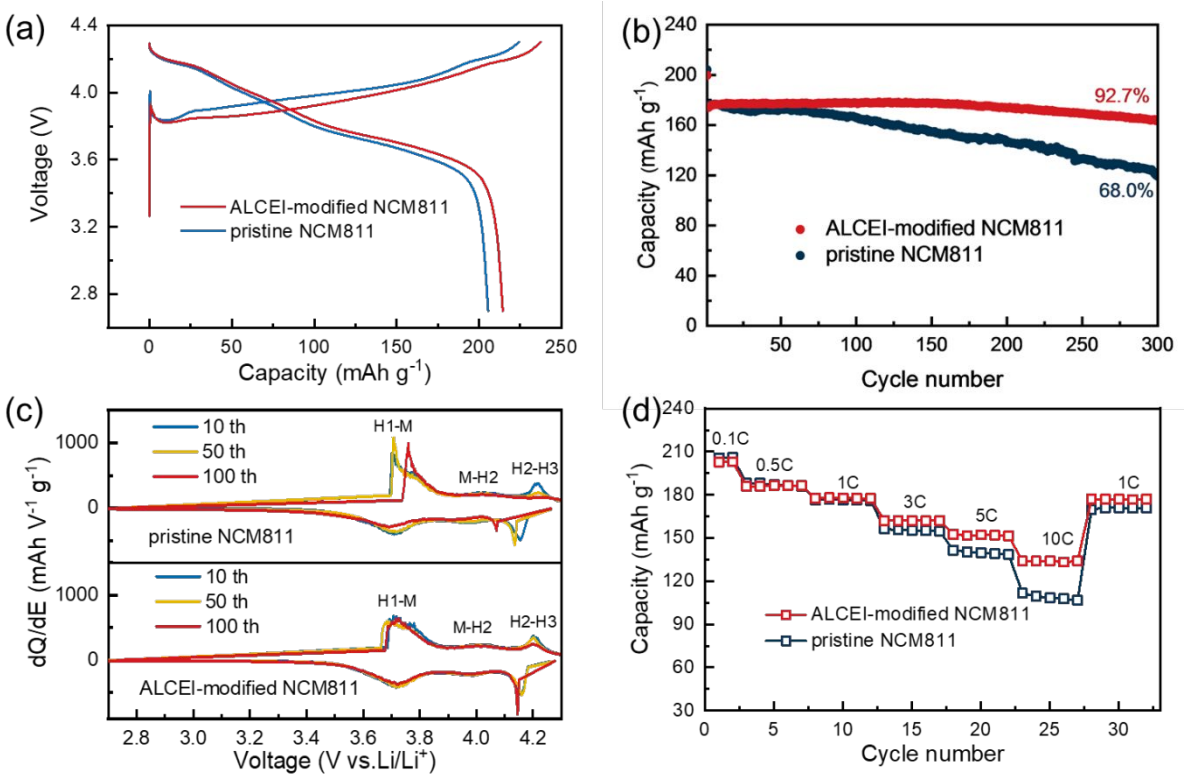

Fig. 5 Electrochemical performances of the pristine and modified NCM811 cathodes: (a) The first charge-discharge curves at 0.1C; (b) Cycling performance at 1C (200 mAh g^{-1}); (c) Differential capacity vs. potential profiles at 10th, 50th, and 100th cycles; (d) Rate performance.

The difference in surface structural stability between pristine and ALCEI-modified NCM811cathodes are also evident in their differential capacity profiles as shown in Figure 5c. Both cathodes exhibit three pairs of redox peaks in their dQ/dV profiles that represent the reversible phase transitions of H1-M, M-H2, and H2-H3 as their CV features. With increasing cycles from the first to 100th cycle, the oxidation peak (H1→M) of pristine cathode positively shifts by 57.7 mV to a higher potential and its corresponding reduction peak negatively shifts by 22.3 mV to a lower potential, demonstrating a gradually increased polarization. Along with the increased polarization, peak intensities are also substantially reduced which indicates gradual capacity decay with increased cycling. However, this electrochemical degradation does not take place on the modified cathode. As the cycle number increases to 10, 50, and 100 cycles all redox peaks remain unchanged in the potential position and intensity, which indicates a very stable electrochemical interface on the ALCEI-modified cathode. Undoubtedly, such a stable interface is brought about by the ALCEI layer, which prevents electrolyte penetration and inhibits parasitic surface reactions, thereby eliminating the surface irreversible phase transition and improving the electrochemical reversibility of the cathode.

The modified NCM811 cathode benefits from the favorable ALCEI layer and exhibits excellent high-rate performance. As shown in Figure 5d, with the current rates increasing from 0.1C to 0.5C, 1C, 3C and 5C, the reversible capacity of the ALCEI-modified cathode slowly decreased from 202 mAh g^{-1} to 186, 178, 162, and 152 mAh g^{-1}, respectively. Even at a very high rate of 10C, the modified cathode can still deliver a high capacity of 134 mAh g^{-1}. Once the current rate returns back to 1C its capacity immediately recovers to 178 mAh g^{-1}, demonstrating a strong high-rate tolerance. In contrast, the pristine cathode capacity of 108 mAh g^{-1} at 10C is much lower.

Electrochemical impedance spectroscopy (EIS) was used to show

electrochemical performance improvements from using ALCEI layers on NCM811 cathode. Figure 6a-c gives the EIS spectra of pristine and ALCEI-modified NCM811 cathodes at 30th, 60th, and 100th cycles. For a convenient comparison all EIS spectra were obtained from the cathodes after charge to 4.3V. As can be seen, all of the EIS spectra are composed of two semicircles and a sloped line, where the semicircle diameter at medium frequency represents the charge transfer resistance (R_{CT}).[53] At all the cycles, the R_{CT} values of pristine cathode are much higher than those of the modified cathode. According to the equivalent circuit given in the inset of Fig. 6a, the R_{CT} values were fitted and the fitting results are given in Fig. 6d. It can be found that as the cycle number increases from 30 to 60 and 100 cycles, R_{CT} values of the pristine cathode rapidly rise from 71.8 to 86.8 and 113.7 Ω, while the R_{CT} value of the ALCEI-modified cathode increases slightly from 18.8 to 41.3 and 58.9 Ω. Therefore, it can be concluded that the ALCEI layer acts to stabilize the NCM811 cathode surface and decreases the charge transfer resistance of Li^+ insertion reaction, thus leading to high capacity, excellent rate capability and long-term cyclability.

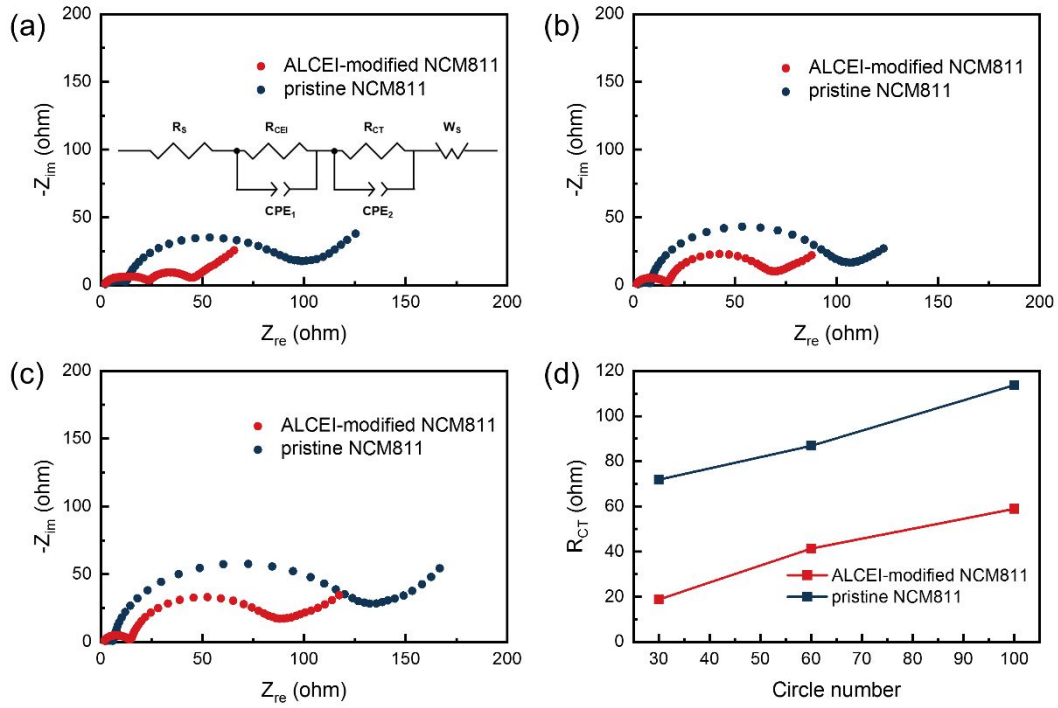

Fig. 6 EIS spectra of the pristine and ALCEI-modified NCM811 cathodes measured at 4.3 V at the (a) 30th, (b) 60th and (c) 100th cycle. (d) Changes in charge-transfer resistances with cycle number.

Asides from creating a stable surface, the ALCEI layer also helps to maintain the morphological integrity of NCM811 cathode. Figure S5 compares the SEM images of the pristine and modified NCM811 cathodes after 40 cycles. As shown in Figure S5a and b, the morphology and structure of the pristine NCM811 particle are seriously damaged and the interconnections among the primary particles are almost disconnected and broken off, which indicates severe electrode degradation. This degradation is undoubtedly caused by the undesirable phase transition. Due to the lack of surface protection, electrolyte can freely penetrate into NCM811 particle interiors and cause the primary particles to undergo irreversible phase transition and the creation of inactive rock-salt phases, which result in particle cracking, fracture, and even pulverization. This should also be responsible for the poor rate and cyclability of the pristine NCM811 cathode. However, with the protection of a modification layer, the modified NCM811 can effectively prevent electrolyte infiltration and preserve structure and morphology during cycling. As demonstrated by the TEM image in Figure S6, the ALCEI layer remains intact and still tightly adheres on the cathode surface after 40 cycles.

4. Conclusions

In summary, we have successfully developed an artificial Li^+-conducting cathode-electrolyte interphase (ALCEI) on the NCM811 cathode surface using a nucleophilic reaction between polysulfides and VC molecules. The as formed ALCEI layer builds a stable electrochemical interface that can not only protect the NCM particles from electrolyte attack but also facilitate Li^+ ion transport across the interface, thus enabling stable and high rate cycling of the Ni-rich cathode. As a result, the ALCEI-modified NCM811 cathode exhibits a high reversible capacity of 211.6 mAh g^{-1} at 0.1C, excellent rate capability at 10C, and superior cycle stability with a 94.2% capacity retention over 200 cycles. These promising results serve to inform the development of cycle stability and high capacity for cathodes in Li ion battery applications.

Author Contributions

Shixuan Wang: Methodology, Visualization, Writing - original draft. **Alvin Dai:** Data curation, Software. **Jun Lu:** Writing - review & editing. **Yuliang Cao:** Supervision. **Hanxi Yang:** Writing - review & editing. **Amine Khalil:** Validation. **Hui Li:** Supervision, Validation. **Xinping Ai:** Conceptualization, Funding acquisition, Supervision, Writing - review & editing.

Conflicts of interest

There are no conflicts to declare.

Acknowledgements

This work was financially supported by International Science and Technology Cooperation of China (2019YFE0100200). Work at Argonne National Laboratory was supported by the U. S. Department of Energy (DOE), Office of Energy Efficiency and Renewable Energy, Vehicle Technologies Office under Clean Vehicles, US-China Clean Energy Research Centre (CERC-CVC2). Argonne National Laboratory is operated for DOE Office of Science by UChicago Argonne, LLC, under contract number DE-AC02-06CH11357.

References

1 Y. Xia, J. Zheng, C. Wang, M. Gu, *Nano Energy,* 2018, **49**, 434-452.
2 H. Zhang, H. Zhao, M. A. Khan, W. Zou, J. Xu, L. Zhang, J. Zhang, *J. Mater. Chem. A,* 2018, **6**, 20564-20620.
3 Y. Ding, D. Mu, B. Wu, R. Wang, Z. Zhao, F. Wu, *Appl. Energy,* 2017, **195**, 586-599.
4 N. S. Choi, Z. Chen, S. A. Freunberger, X. Ji, Y. K. Sun, K. Amine, G. Yushin, L. F. Nazar, J. Cho, P. G. Bruce, *Angew. Chem. Int. Ed.,* 2012, **51**, 9994-10024.
5 M. Li, J. Lu, Z. Chen, K. Amine, *Adv. Mater.,* 2018, **30**, 1800561.
6 S.-T. Myung, F. Maglia, K.-J. Park, C. S. Yoon, P. Lamp, S.-J. Kim, Y.-K. Sun, *ACS Energy Lett.,* 2016, **2**, 196-223.
7 W. Liu, P. Oh, X. Liu, M. J. Lee, W. Cho, S. Chae, Y. Kim, J. Cho, *Angew. Chem. Int. Ed.,* 2015, **54**, 4440-4457.
8 H.-J. Noh, S. Youn, C. S. Yoon, Y.-K. Sun, *J. Power Sources,* 2013, **233**, 121-130.
9 D. Becker, M. Borner, R. Nolle, M. Diehl, S. Klein, U. Rodehorst, R. Schmuch, M. Winter, T. Placke, *ACS Appl. Mater. Interfaces,* 2019, **11**, 18404-18414.
10 H.-H. Ryu, K.-J. Park, C. S. Yoon, Y.-K. Sun, *Chem. Mater.,* 2018, **30**, 1155-1163.
11 H. Yang, H. H. Wu, M. Ge, L. Li, Y. Yuan, Q. Yao, J. Chen, L. Xia, J. Zheng, Z. Chen, J. Duan, K. Kisslinger, X. C. Zeng, W. K. Lee, Q. Zhang, J. Lu, *Adv. Funct. Mater.*, 2019, **29**, 1808825.
12 H. J. Song, S. H. Jang, J. Ahn, S. H. Oh, T. Yim, *J. Power Sources,* 2019, **416**, 1-8.
13 S. Hwang, S. M. Kim, S.-M. Bak, B.-W. Cho, K. Y. Chung, J. Y. Lee, W. Chang, E. A. Stach, *ACS Appl. Mater. Interfaces*, 2014, **6**, 15140-15147.
14 L. Wu, K.-W. Nam, X. Wang, Y. Zhou, J.-C. Zheng, X.-Q. Yang, Y. Zhu, *Chem. Mater.*, 2011, **23**, 3953-3960.
15 C. Liang, F. Kong, R. C. Longo, S. Kc, J.-S. Kim, S. Jeon, S. Choi, K. Cho, *J. Phys. Chem.* C, 2016, **120**, 6383-6393.
16 S. S. Zhang, *Energy Storage Mater.,* 2020, **24**, 247-254.
17 H. Maleki Kheimeh Sari, X. Li, *Adv. Energy Mater.,* 2019, **9**, 1901597.
18 K. Min, E. Cho, *Phys. Chem. Chem. Phys.,* 2018, **20**, 9045-9052.
19 X. Wang, J. Cai, Y. Liu, X. Han, Y. Ren, J. Li, Y. Liu, X. Meng, *Nanotechnology,* 2020, **32**, 115401.
20 K. Min, C. Jung, D. S. Ko, K. Kim, J. Jang, K. Park, E. Cho, *ACS Appl. Mater. Interfaces,* 2018, **10**, 20599-20610.
21 B.-J. Chae, J. H. Park, H. J. Song, S. H. Jang, K. Jung, Y. D. Park, T. Yim, *Electrochim. Acta*, 2018, **290**, 465-473.
22 X. He, X. Xu, L. Wang, C. Du, X. Cheng, P. Zuo, Y. Ma, G. Yin, J. *Electrochem. Soc.,* 2019, **166**, A143-A150.
23 S. Chen, T. He, Y. Su, Y. Lu, L. Bao, L. Chen, Q. Zhang, J. Wang, R. Chen, F. Wu, *ACS Appl. Mater. Interfaces*, 2017, **9**, 29732-29743.
24 T. Weigel, F. Schipper, E. M. Erickson, F. A. Susai, B. Markovsky, D. Aurbach, *ACS Energy Lett.,* 2019, **4**, 508-516.
25 J. Chen, H. Yang, T. Li, C. Liu, H. Tong, J. Chen, Z. Liu, L. Xia, Z. Chen, J. Duan, L. Li, *Front. Chem.*, 2019, **7**, 500.
26 Y. K. Sun, S. T. Myung, B. C. Park, J. Prakash, I. Belharouak, K. Amine, *Nat. Mater.*, 2009, **8**, 320-324.
27 H.-J. Noh, S.-T. Myung, Y. J. Lee, Y.-K. Sun, *Chem. Mater.*, 2014, **26**, 5973-5979.
28 H. Li, J. Li, X. Ma, J. R. Dahn, *J. Electrochem. Soc.*, 2018, **165**, A1038-A1045.
29 T. Yim, S. H. Jang, Y.-K. Han, *J. Power Sources,* 2017, **372**, 24-30.
30 G. Lan, L. Xing, D. Bedrov, J. Chen, R. Guo, Y. Che, Z. Li, H. Zhou, W. Li, *J. Alloy. Compd.,* 2020, **821**, 153236.
31 K. Beltrop, S. Klein, R. Nölle, A. Wilken, J. J. Lee, T. K. J. Köster, J. Reiter, L. Tao, C. Liang, M. Winter, X. Qi, T. Placke, *Chem. Mater.*, 2018, **30**, 2726-2741.
32 P. Karayaylali, R. Tatara, Y. Zhang, K.-L. Chan, Y. Yu, L. Giordano, F. Maglia, R. Jung, I. Lund, Y. Shao-Horn, *J. Electrochem. Soc.*, 2019, **166**, A1022-A1030.
33 L. Yao, F. Liang, J. Jin, B. V. R. Chowdari, J. Yang, Z. Wen, *Chem. Eng. J.,* 2020, **389**, 124403.
34 S. Neudeck, A. Mazilkin, C. Reitz, P. Hartmann, J. Janek, T. Brezesinski, *Sci. Rep.,* 2019, **9**, 5328.
35 X. Xiong, Z. Wang, X. Yin, H. Guo, X. Li, *Mater. Lett.,* 2013, **110**, 4-9.
36 C. M. Julien, A. Mauger, *AIMS Mater. Sci.,* 2019, **6**, 406-440.
37 W. Cho, S.-M. Kim, K.-W. Lee, J. H. Song, Y. N. Jo, T. Yim, H. Kim, J.-S. Kim, Y.-J. Kim, *Electrochim. Acta*, 2016, **198**, 77-83.
38 W. Tang, Z. Peng, Y. Shi, S. Xu, H. Shuai, S. Zhou, Y. Kong, K. Yan, T. Lu, G. Wang, *J. Power Sources,* 2019, **810**, 151834.
39 P. Zou, Z. Lin, M. Fan, F. Wang, Y. Liu, X. Xiong, *Appl. Surf. Sci.,* 2020, **504**, 144506.
40 Q. Gan, N. Qin, Z. Wang, Z. Li, Y. Zhu, Y. Li, S. Gu, H. Yuan, W. Luo, L. Lu, Z. Xu, Z. Lu, *ACS Appl. Energ. Mater.*, 2020, **3**, 7445.
41 [41] Z. Zhong, L. Chen, C. Zhu, W. Ren, L. Kong, Y. Wan, J. Power Sources 2020, 464, 228235.
42 J. Chen, L. Zhu, D. Jia, X. Jiang, Y. Wu, Q. Hao, X. Xia, Y. Ouyang, L. Peng, W. Tang, T. Liu, *Electrochim. Acta,* 2019, **312**, 179-187.
43 X. Qu, Z. Yu, D. Ruan, A. Dou, M. Su, Y. Zhou, Y. Liu, D. Chu, *ACS Sustain. Chem. Eng.,* 2020, **8**, 5819-5830.
44 Y. Shi, L. Peng, Y. Ding, Y. Zhao, G. Yu, *Chem. Soc. Rev.,* 2015, **44**, 6684-6696.
45 S. Xu, C. Du, X. Xu, G. Han, P. Zuo, X. Cheng, Y. Ma, G. Yin, *Electrochim. Acta,* 2017, **248**, 534-540.
46 X. Xiong, D. Ding, Z. Wang, B. Huang, H. Guo, X. Li, *J. Solid State Electrochem.,* 2014, **18**, 2619-2624.
47 F. He, X. Wu, J. Qian, Y. Cao, H. Yang, X. Ai, D. Xia, *J. Mater. Chem. A,* 2018, **6**, 23396-23407.
48 M. S. Park, H. S. Woo, J. M. Heo, J. M. Kim, R. Thangavel, Y. S. Lee, D. W. Kim, *ChemSusChem,* 2019, **12**, 4645-4654.

49 S. Grugeon, P. Jankowski, D. Cailleu, C. Forestier, L. Sannier, M. Armand, P. Johansson, S. Laruelle, *J. Power Sources,* 2019, **427**, 77-84.

50 A. L. Michan, B. S. Parimalam, M. Leskes, R. N. Kerber, T. Yoon, C. P. Grey, B. L. Lucht, *Chem. Mater.,* 2016, **28**, 8149-8159.

51 R. Robert, C. Bünzli, E. J. Berg, P. Novák, *Chem. Mater.,* 2015, **27**, 526-536.

52 Q. Gan, N. Qin, Y. Zhu, Z. Huang, F. Zhang, S. Gu, J. Xie, K. Zhang, L. Lu, Z. Lu, *ACS Appl. Mater. Interfaces,* 2019, **11**, 12594-12604.

53 Y.-Y. Sun, S. Liu, Y.-K. Hou, G.-R. Li, X.-P. Gao, *J. Power Sources,* 2019, **410-411**, 115-123.